EPIDEMIOLOGY

Collateral effects of COVID-19 pandemic control on the US infectious disease landscape

Tobias S. Brett[1]* and Pejman Rohani[1,2,3]

Using data from the United States Centers for Disease Control and Prevention (CDC) disease surveillance systems, we sought to quantify the indirect effects of the COVID-19 pandemic, and the possibility of lack of exposure to common pathogens resulting in immune deficits. Clustering analysis on pandemic-era time-series data identified pathogen groupings according to transmission mechanism. Counterfactual analysis, using Bayesian structural time-series (BSTS) modeling, confirmed that infectious diseases that are directly transmitted via airborne droplets (aerosols) experienced the greatest disruption to transmission. By contrast, sexually transmitted infections (STIs) experienced a smaller transient disruption, and increasing trends in incidence prepandemic appear to have been curtailed. Using epidemiological theory, we demonstrate that the observed magnitudes and durations of notifications deficits were determined by fundamental disease system properties, namely, the serial interval, basic reproductive number, and susceptible recruitment.

The COVID-19 pandemic, caused by the emergence of the novel severe acute respiratory syndrome coronavirus 2 (SARS-CoV-2) coronavirus (*1*), triggered an unprecedented global disruption to human society. Although governmental response measures and individual behavioral changes were targeted at curtailing the spread of SARS-CoV-2 (*2*), they also influenced co-circulating, sympatric infectious diseases (*3*–*10*). Of particular concern was the prospect that the implementation of social distancing measures would lead to gaps in population immunity against these diseases, with the potential for serious rebound in incidence for some infections after the relaxation of control measures (*11*–*15*). These fears, motivated by epidemiological theory (*16*, *17*), were borne out in part by the "triple-demic" of SARS-CoV-2, respiratory syncytial virus (RSV), and influenza virus (Fig. 1, A and B) during the winter of 2022–2023 (*18*) and may be contributing to a resurgence of pertussis in 2024 and 2025 (Fig. 1D) (*19*). Additional concerns were raised about potential disruption to disease surveillance efforts, routine vaccination programs (*20*), patient care–seeking behavior (*21*), and health care system capacity (*22*). Ecological competition by a novel pathogen may also have disrupted the community of human infectious diseases (*23*, *24*). The interpretation of post-COVID disease incidence trends is complicated by pandemic-spurred improvements in disease surveillance methodologies (*25*, *26*), spatial variation in disease incidence, and state government responses (Fig. 1, E to J).

The short-term effects of social distancing measures on sympatric infectious diseases have been examined for specific pathogens, including influenza (*11*, *27*, *28*), RSV (*11*, *29*), polio (*30*), tuberculosis (*31*, *32*), pertussis (*10*, *33*, *34*), and enterovirus D68 (*35*). Though valuable in providing epidemiological insights, most of these studies were performed at the height of the pandemic (2020–2021) with the aim of providing "scenario analyses" to project possible postpandemic implications for specific pathogens and diseases. Here, we present a retrospective analysis of surveillance data spanning the pandemic, with the aim of identifying patterns in the impacts of pandemic response measures on a suite of sympatric infectious diseases in the USA.

We carried out a comparative study using time-series data collected by the US Centers for Disease Control and Prevention and made publicly available through the National Notifiable Disease Surveillance System (NNDSS) and FluView (*36*, *37*). From the two sources, we collated a dataset of 24 infectious diseases amenable to statistical analysis.

Clustering analysis

To identify which groupings of diseases were similarly affected by the COVID-19 pandemic, we performed a clustering analysis on the national-level weekly notifications data from the start of 2019 onwards (Fig. 2; full time-series data are shown in fig. S1). We calculated the Spearman's ρ rank-correlation matrix, finding values of ρ that ranged from −0.47 (between syphilis and mumps) to 0.91 [between campylobacteriosis and Shiga toxin–producing *Escherichia coli* (STEC)] (Fig. 2A). We applied an agglomerative clustering algorithm to the correlation matrix, to construct a dendrogram of the hierarchical clustering of the data (Fig. 2B). On the basis of the silhouette score (fig. S2), we found that the data were most consistent with four clusters.

The clustering is suggestive of factors that might have helped shape the pandemic's effects on disease transmission (Fig. 2). The first cluster (shaded blue) comprises predominantly pathogens that are spread via airborne or aerosol transmission (with hepatitis B, spread by infected blood or bodily fluids, an outlier); one subgroup consists of vaccine-preventable childhood diseases (mumps, pertussis, invasive *H. influenzae*, and varicella) and the other, influenza A and B. The second (shaded pink) consists of the three sexually transmitted infections (STIs) in the dataset (gonorrhea, chlamydia, and syphilis), with coccidioidomycosis (environmentally transmitted) being an outlier. The third (shaded green) is more disparate but broadly consists of diseases that are not directly transmissible between humans, with one subgrouping consisting of bacteria spread fecal-orally (with malaria an outlier) and a second subgroup of tick-borne pathogens. The final group consists of two apparent outliers: hepatitis A, caused by a virus primarily spread primarily via fecal-oral transmission [which experienced a pronounced multistate outbreak from 2016 to 2019 (*38*)], and notifications of rabies in animals [the only nonhuman disease in the dataset, included for comparative purposes, which is subject to an ongoing vaccination campaign (*39*)]. In what follows, we will focus on the first three clusters, which we label according to predominant transmission mechanism: (i) airborne and aerosol-transmitted infections (ATIs), (ii) STIs, and (iii) environmentally transmitted infections and zoonotic spillover (ETI/Z). To verify that the clustering corresponds to effects of the pandemic and not prepandemic patterns, we repeated the clustering analysis using data pre-2020 (fig. S3). The resulting dendrogram was less reflective of transmission mechanism, although some features were preserved based on seasonal patterns of incidence (e.g., the STI cluster and a high correlation between influenza A and B).

Counterfactual analysis

To quantify the effects of the pandemic on sympatric disease notifications in different US states, we performed a counterfactual Bayesian structural time-series (BSTS) modeling analysis (*40*). The analysis was designed to estimate the discrepancy between observed notifications post-March 2020 and the counterfactual projected notifications predicted to have occurred had no pandemic taken place (see materials and methods). We fit the BSTS model to time-series data for each pairwise combination of US state and disease. Model validation was performed using posterior predictive checks, with 298 pairs passing the check (fig. S4).

[1]Odum School of Ecology, University of Georgia, Athens, GA, USA. [2]Department of Infectious Diseases, College of Veterinary Medicine, University of Georgia, Athens, GA, USA. [3]Center for Influenza Disease and Emergence Research (CIDER), Athens, GA, USA. *Corresponding author. Email: tsbrett@uga.edu

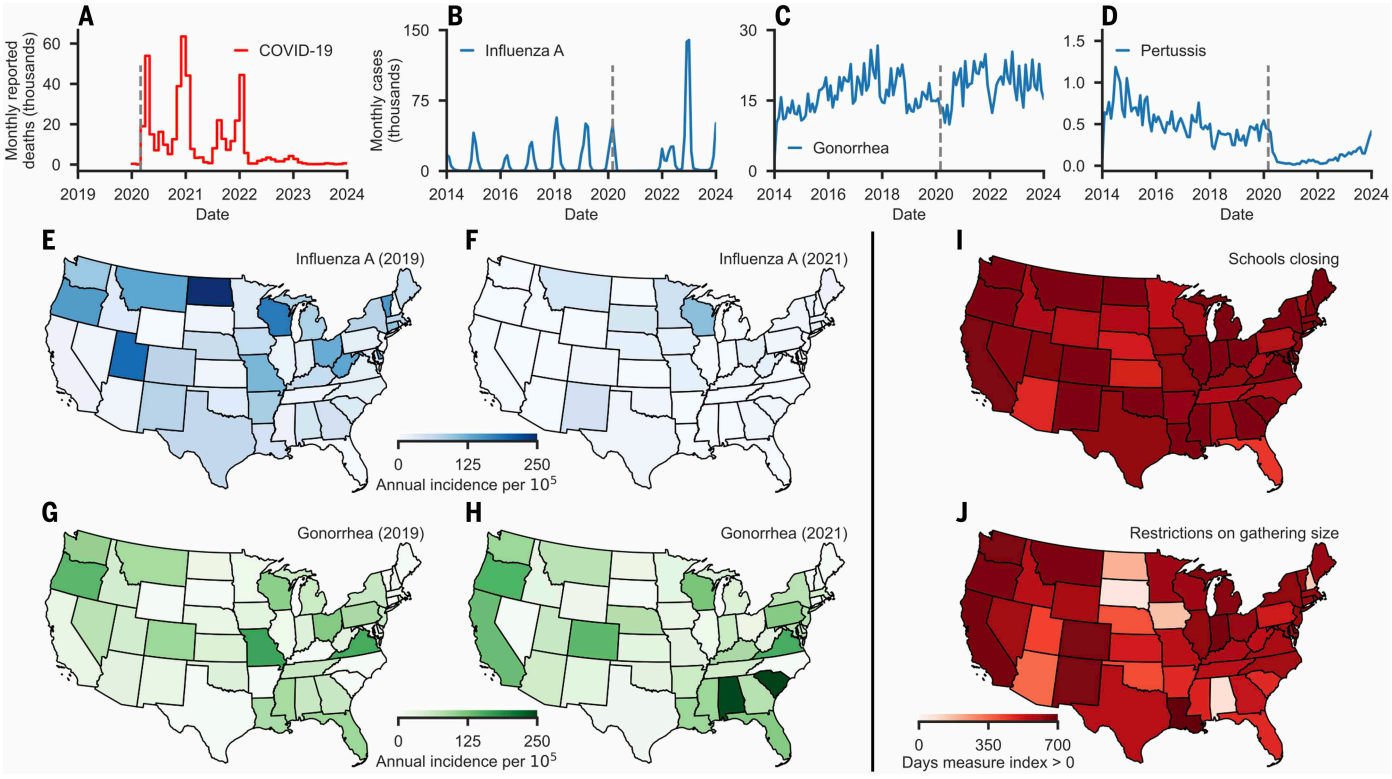

Fig. 1. Overview of pre– and post–COVID-19 notifications for select diseases. (**A**) Monthly recorded COVID-19 mortality. (**B** to **D**) Monthly notifications of cases of influenza A (B) gonorrhea (C), and pertussis (D). (**E** to **H**) On the state level, differences in notifications of influenza A were consistently lower in 2021 compared with 2019 (E and F). By contrast, changes in notifications of gonorrhea varied by state with some up (e.g., Alabama, California, South Carolina) and others down (e.g., Missouri, Nevada, Ohio). (**I** and **J**) The duration of government response measures also varied by state, as quantified by the Oxford COVID-19 Government Response Tracker (OxCGRT; see materials and methods). Although some level of disruption to education in schools remained across much of the country for almost 2 years (I), restrictions on gathering sizes were relaxed more quickly, and with greater spatial variation (J).

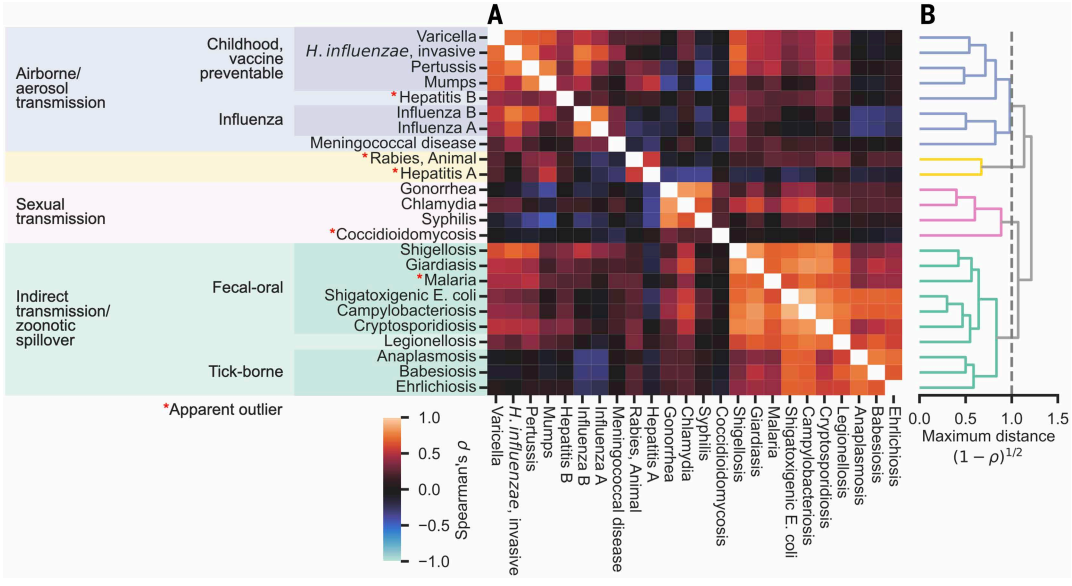

Fig. 2. Clustering analysis of sympatric disease time-series data from the US (2019–2024). (**A**) Spearman's rank correlation matrix for time-series data of weekly national case notifications for 24 infectious diseases (22 from the NNDSS plus lab-confirmed influenza A and B cases; see materials and methods). (**B**) Agglomerative clustering algorithm (*55*) applied to the correlation matrix, with the silhouette score (*56*) identifying four distinct clusters (fig. S2). Of these clusters, one (blue) primarily consists of airborne and aerosol-transmitted infections (ATIs). The second (pink) is of predominantly STIs. The third (green) is a broad cluster, which we label ETI/Z, that includes zoonotic tick-borne infections (anaplasmosis, babesiosis, and ehrlichiosis) and environmentally transmitted infections (ETIs). Diseases in this cluster do not depend on direct human contact for transmission. The final cluster (yellow) consists of two outliers, hepatitis A and rabies in animals.

The key measure used to interpret our results was the relative impact on disease notifications, ψ_t, given by $\psi_t = 100(y_t - \tilde{y}_t) / \tilde{y}_t$, which quantifies, as a percentage, the deviation of observed notifications y_t from counterfactual model projections, $\tilde{y}_t$ (Fig. 3, A and B). Similarly, the relative net impact, $\chi_t = 100 \sum_{s=0}^{t} (y_s - \tilde{y}_s) / \sum_{s=0}^{t} \tilde{y}_s$, quantifies the cumulative deviation of observed notifications from counterfactual model projections from the start of the pandemic up to time t. Related approaches have previously been used to quantify excess deaths attributable to the pandemic (*41*).

In Fig. 3, C to J, we present results for four diseases in New York state, representative of the three transmission clusters (Fig. 2A). Results for all other state-disease pairs are presented in figs. S5 to S10. In 2020, notifications of both influenza A (Fig. 3G) and pertussis (Fig. 3H) were substantially below counterfactual projections (posterior median annual relative annual impact −81.5% [−90.5%, −69.7%] and −76.6% [−81.8%, −71.2%], respectively), whereas the relative annual impact on shigellosis notifications (Fig. 3J) was −45.7% [−55.7%, −34.5%]; all ranges correspond to 95% highest density intervals (HDIs). Notifications of all three diseases subsequently rebounded with the annual relative impact 95% HDI containing 0% by the end of 2022. The return of both pertussis and shigellosis to projected levels has been gradual over the course of 2020–2022 (although there were explosive outbreaks of pertussis in New York during 2024, among other locations). By contrast, influenza A was largely absent until a sudden rebound in 2022 (Fig. 3G). Unlike the other three diseases shown, there was no apparent effect on weekly gonorrhea notifications in 2020 (Fig. 3I), with a relative annual impact of −1.2% [−8.5%, 6.5%], although notification reports were absent from early July until late November 2020. Subsequently, there was a small negative impact in 2022 and 2023, as notifications undershot projections that sustained an increasing pre-2020 trend. For all four diseases shown (Fig. 3, G to J), the relative net impact remains below zero at the end of 2023, corresponding to a net deficit in notifications.

Given the large number of state-disease pairs, we summarized our results by aggregating estimates of the relative net impact on each pathogen for each cluster (Fig. 4). We found that the median for all three clusters (with influenza excluded from the ATI cluster) remained below zero at the end of 2023 (Fig. 4A). Although following a similar trajectory to other ATIs, both influenza A and B were most influenced by the pandemic during 2021 (Fig. 4B). Subsequently, during 2022 and 2023, the influenza A rebound was positive in some states (in particular South Dakota, Hawaii, and Nebraska), whereas in others, the influenza seasons were smaller than expected (e.g., Michigan and Louisiana; fig. S11). By contrast, at the start of 2024, influenza B was suppressed in all states apart from Mississippi and South Carolina (fig. S12).

Broadly speaking, the effect of the pandemic and related response measures on other pathogens appears to be more strongly shaped by transmission mechanism of the pathogen concerned than state-level effects (Fig. 4, C to E). To understand whether state-specific differences in COVID-19 response measures could explain the interstate variation in the relative net impact on other pathogens, we formulated a multilevel regression model that we fit to predict the median relative net impact at the end of 2021, 2022, and 2023 using a dataset of government response measures as predictors (figs. S13 to S16). Except for the school closure coefficient for the ATI cluster, the posterior 95% HDI for each coefficient in 2021 included zero (fig. S14B). This indicates that our model was unable to use those predictors to explain interstate variation in relative net impact (χ_t). Our results do not imply that those response measures made no contribution to χ_t, given that the data were standardized and that we estimated nonzero offsets for

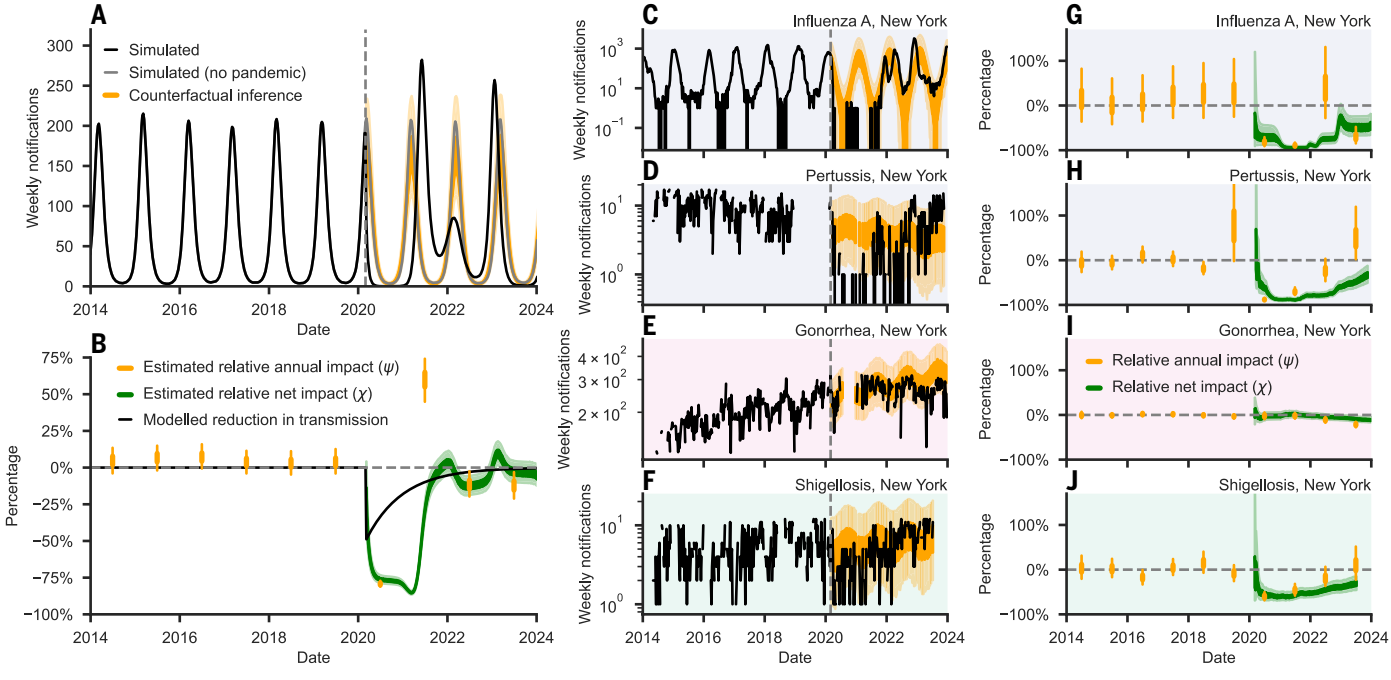

Fig. 3. Results of the counterfactual inference analysis for four diseases in New York. (**A**) Demonstration of counterfactual approach using simulated data. The model was fit to data pre-March 2020, with counterfactual projections (which assumed no pandemic effects) made for subsequent weeks. The counterfactual projections agree with simulated data that assumed no pandemic (gray line) but deviated from the simulated trajectory that assumed an initial 50% reduction in transmission. (**B**) The discrepancy between data post-2020 and the counterfactual projections allow us to quantify the relative impact, which lags the modeled reduction in transmission. Orange intervals show the relative annual impact for a given calendar year; green ribbons show the cumulative relative net impact since the pandemic start (dark and light bars/ribbons correspond to the 50% and 95% HDI, respectively). (**C** to **F**) Weekly observed notifications of influenza A, pertussis, gonorrhea, and shigellosis (black) are compared with counterfactual predictions from the BSTS model. (**G** to **J**) Relative annual and net impact of the pandemic. The annual impact calculations for 2020 only include data post-March.

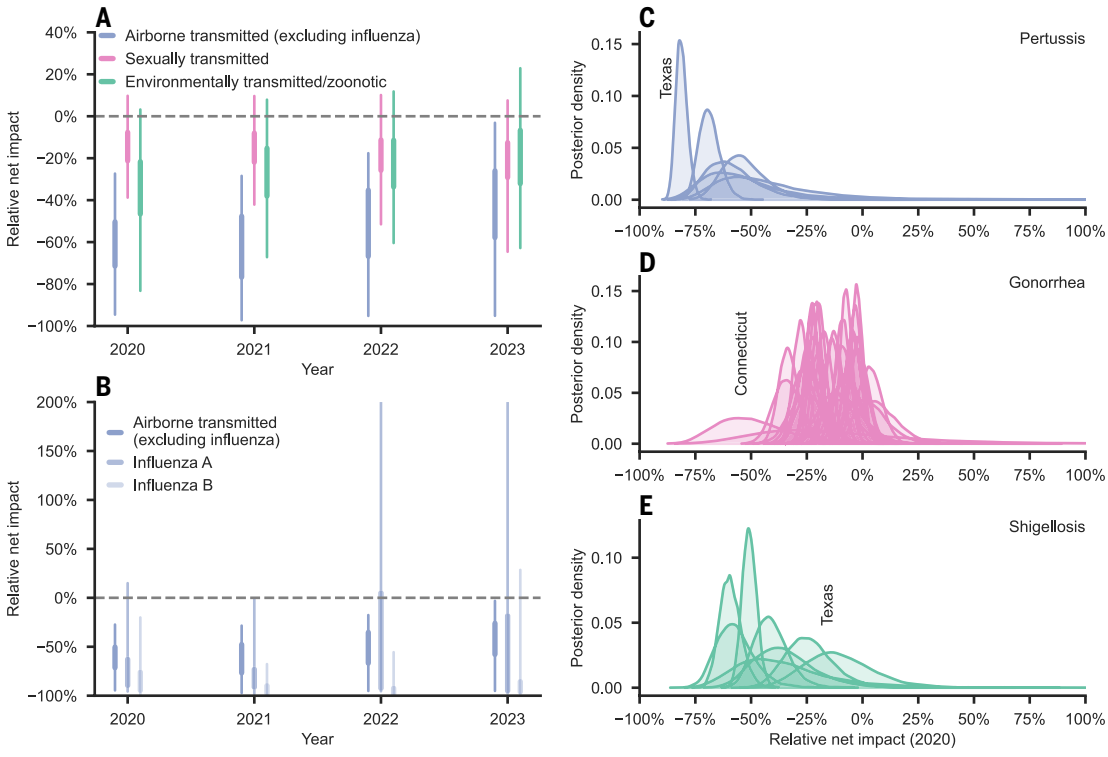

Fig. 4. Relative net impact by year and cluster. (**A**) Relative net impact at the end of each year for each transmission cluster. Densities computed by aggregating posterior samples for all state-disease pairs in a cluster (points indicate the median; bars correspond to 50% and 95% HDIs). Owing to the atypical relative net impact on influenza, we excluded it from the ATI cluster. (**B**) Comparison of the relative net impact on influenza with the rest of the ATI cluster diseases, using the same approach as for (A). For influenza A, the 95% HDI extends to 424% and 435% in 2022 and 2023, respectively. (**C** to **E**) State-level variation in relative net impact for pertussis (C), gonorrhea (D), and shigellosis (E).

each cluster (fig. S14C). Qualitatively similar results were observed for both 2022 and 2023 (figs. S15 and S16).

To explore the possible mechanisms underlying the differences between the two directly transmitted clusters (ATIs and STIs), we formulated and analyzed a simple pathogen transmission model (see materials and methods for details). We modeled the pandemic as causing a reduction in the transmission rate, which followed a decaying exponential, $c(t) = c_0\left(1-e^{-t/\tau}\right)$, where c_0 is the reduction at the start of the pandemic and τ determines the rate of return to the prepandemic transmission level (Fig. 5A). Following the methodology of our counterfactual analysis, we calculated the relative net impact and the return time, defined as the mean time for the relative net impact to return within 10% of zero. Using plausible parameter values, we simulated three diseases: pertussis (Fig. 5, B and C), influenza A (Fig. 5, D and E), and gonorrhea (figs. S17 and S18). We also simulated a set of parameter scenarios (Fig. 5H and figs. S19 and S20). For pertussis, we see a return time of about 4 years, followed by decaying oscillations in the net impact. For influenza, we see greater variation between stochastic replicates, with the net impact returning to zero after about 1 to 2 years. Basic epidemiological theory can explain the observed dynamics. Early in the pandemic, prevalence drops exponentially, $\frac{dI(t)}{dt} \approx -c_0\gamma I(t)$, depending on the severity of control measures, c_0, and the pathogen infectious period, $1/\gamma$. Later, as the transmission rate approaches prepandemic levels, the rebound is shaped by the basic reproductive number, R_0, and the rate of influx into the susceptible pool, κ, approximately following $\frac{dI(t)}{dt} \approx \gamma\kappa R_0 I(t)$. The parameter κ comprises the rate of unvaccinated births and loss of infection- and vaccine-derived immunity. Seasonal infectious diseases with low basic reproductive number, short infectious period, and short-lived immunity, such as influenza, are expected to undergo a sharp decline followed by a volatile rebound before returning to zero. These patterns are broadly in line with observations for influenza A (fig. S11). The return time is sensitive to nonlinearities in the transmission process, analogous to period doubling observed for vaccine-controlled seasonal diseases (*42*). For gonorrhea, we find that the observed relative net impact (for instance in New York; Fig. 3I) is most consistent with a smaller effect of the pandemic compared to the ATIs (both in the magnitude and duration of reductions in transmission rates; fig. S17). Furthermore, to match trends in the data, our modeling required that an increasing trend in transmission rates pre-2020 ended at the start of the COVID-19 pandemic.

Discussion

A limitation of counterfactual analyses is the assumption that data trends can be extrapolated from the training period (the prepandemic period in our study) into the counterfactual projection period (i.e., after March 2020). Therefore, a major caveat to the findings of our BSTS analysis is that it cannot, in isolation, distinguish between effects of the pandemic and other coincidental secular trends in transmission dynamics and surveillance after 2020. For instance, contemporary patterns of incidence may be affected by factors unrelated to the pandemic period, including changes in diagnostic methodology [e.g., increased usage of multiplex assays (*25*, *26*)], behavior [e.g., vaccine hesitancy (*43*)], and pathogen transmissibility and virulence (*44*). Another limitation is our choice of model structure. Given the large number of diseases studied, we opted to use a generalized linear model; however, appropriate disease-specific mechanistic transmission models could provide better interpretations of the data. Furthermore, as we were fitting to 6 years of data pre-2020, diseases with long interepidemic periods [such as mumps (*45*)] were difficult to fit with

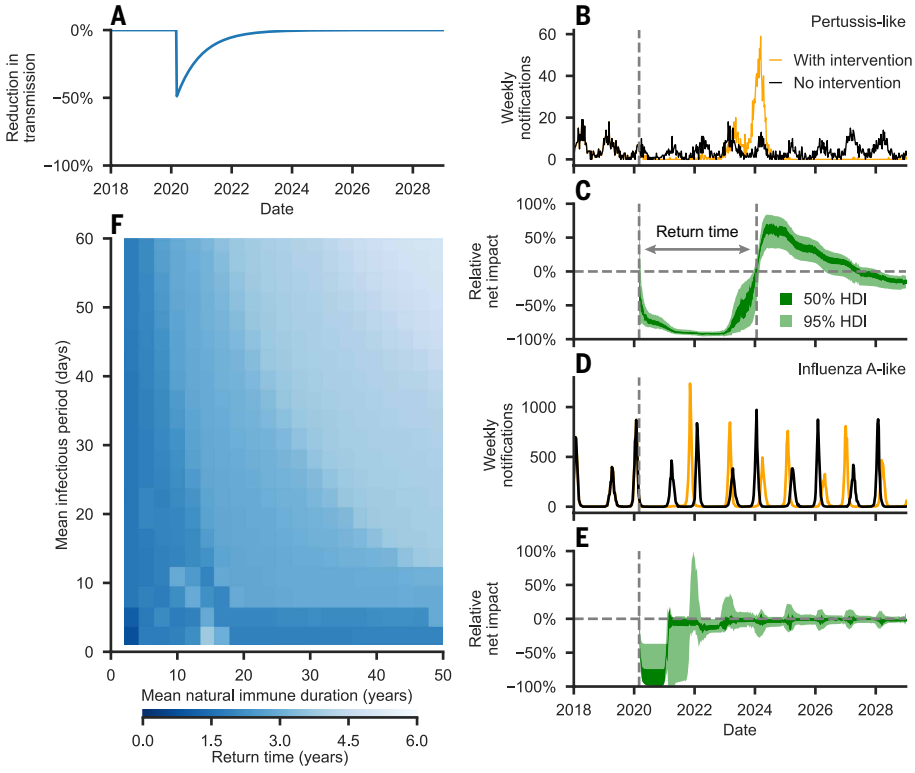

Fig. 5. Scenario analysis. (**A** to **E**) Simulated results using a stochastic SEIRV model (see materials and methods) subject to an initial 50% reduction in transmission rates (A). Results shown using plausible parameterizations for two ATIs, pertussis (B and C) and influenza A (D and E). (**F**) Dependence of the return time on the natural immune duration and infectious period for a pathogen with $R_0 = 4$. The return time was defined as the duration between the start of control measures and the mean relative net impact crossing −10% (C).

our nonmechanistic model. For instance, mumps and hepatitis A experienced pronounced outbreaks in several states during the prepandemic period (2014–2020), which led to rejection under statistical inclusion criteria (see materials and methods).

Our counterfactual analysis shows that notifications of some of the infectious diseases being investigated, in particular STIs, were largely unaffected by the pandemic (Fig. 4). From this observation, we infer that there was no generalized collapse in disease surveillance during the acute phase of the pandemic, and decreases in notifications of other diseases likely reflect actual reductions in transmission. Nevertheless, we cannot rule out the possibility of disproportionate disruption to the surveillance of specific diseases or in specific states.

The limited effect on notifications of the three STIs during 2020 and 2021 is puzzling, given the severe lockdown measures imposed and their effect on SARS-CoV-2 and ATI transmission. Our analysis of a gonorrhea-like transmission model suggests that even a moderate (initially 25%) short-lived reduction in transmission rates should have had a greater discernible net impact than observed for most state-disease pairs in the STI cluster (fig. S17). The longer serial interval of STIs relative to ATIs alone cannot explain the limited drop in notifications during 2020 (figs. S17 to S20). Another unexplained observation in these data (2014–2024) is that increasing trends in notifications that predated the pandemic have been absent since 2020, a phenomenon repeated across states and STIs in the study. Our results point to a persistent change in STI transmission dynamics that appears to us unexplained.

It is not surprising that ATIs were most affected by the pandemic, given the types of recommended control measures (e.g., mask wearing, reductions in mass gatherings, school and workplace closures) that were implemented to stop the spread of an aerosol-transmitted virus such as SARS-CoV-2. However, the delay in the rebound of these infectious diseases is noteworthy. For instance, in the US, despite public health interventions, contact rates were still sufficient for the rapid spread of the alpha, delta, and omicron variants in 2021 and influenza A in winter 2022 (*46*). By contrast, over the same period, the incidence of influenza B, invasive *H. influenzae*, mumps, pertussis, and varicella all remained below expected levels. Epidemiological modeling indicated a number of possible mechanisms (Fig. 5 and fig. S19). Specifically, the suppressed infectious diseases have longer serial intervals (resulting in slower epidemiological growth rates), lower transmissibility, and longer durations of immunity (and therefore slower susceptible recruitment). Regardless of parameterization, our modeling suggests that the effect of the pandemic is unlikely to extend beyond about 6 years. Our results point to a need for more systematic study of the underlying mechanisms. Indeed, the disruptive effects of the pandemic on the circulation of other infectious diseases provides a valuable opportunity to better understand the epidemiology of these pathogens.

Of the ATIs, it is not clear why influenza A and B notifications were disproportionately affected (Fig. 4B). Perhaps this is a result of disrupted international travel, which is known to play an important role in the circulation and seeding of novel influenza antigenic variants (*47*, *48*); however, curiously, influenza A was less affected by this perturbation than influenza B, despite the higher frequency of variant introductions before the pandemic (*48*). Alternatively, viral interference after SARS-CoV-2 infection and vaccination may have affected sympatric viruses (*49*). Apart from SARS CoV-2, influenza viruses are the only viruses in our study that infect the respiratory tract; therefore, it is possible that they experienced the greatest interference from the emergence of SARS-CoV-2.

Our quantification of the pandemic's impact has focused on the USA, where SARS-CoV-2 has circulated continuously since early 2020. However, the pandemic left a qualitatively similar footprint on notifications data for influenza in Australia (fig. S21) and pertussis in New Zealand (fig. S22), countries that adopted a zero-COVID strategy and largely suppressed SARS-CoV-2 circulation until late 2021. Timing of interventions relative to epidemic phase was found to affect the return time, with simulations where transmission reductions coincided with the start of the epidemic season demonstrating longer disruption (fig. S20).

Our findings are consistent with available studies of other populations [US military personnel (*50*)] and disease systems [*Salmonella* in Germany (*51*)]. An intriguing study of seasonal endemic respiratory viruses in Washington state, including a number of viruses not part of the NNDSS, found that the non-enveloped viruses in the study (human rhinoviruses, enteroviruses, and adenoviruses) were the first to rebound after the lifting of lockdown measures (*52*). The authors speculate that virological factors, such as environmental stability and ability to penetrate face masks, may have facilitated their rapid spread. Alternatively, our results suggest that short serial intervals and short-lasting immunity ($\lesssim$ 2 years) are sufficient to explain their rapid rebound.

In 2025, notifications of the ATIs largely rebounded to prepandemic levels as expected (*11*, *13*). It was unclear whether the rebound in these

diseases would exceed the incidence prevented by pandemic control measures, owing to the immunity gap created by reduced pathogen circulation and missed routine vaccinations. Our results show that cumulative notifications of most ATIs in most states since 2020 remained at a net deficit compared with counterfactual projections at the start of 2024. Given that we do not find evidence for a substantial collapse in disease reporting during 2020, we expect this deficit to reflect an overall reduction in the burden of disease. Although governmental-response measures to control the pandemic undoubtedly had adverse psychological, economic, and societal consequences (*53*), considered solely through the lens of infectious disease notifications, lockdown measures were beneficial for human health and did not lead to a collateral excess of sympatric disease. Extrapolating from disease notifications to the total number of infections in the population, and the implications for population immunity, can only be done on a disease-by-disease basis and remains a pressing need for further study such as through serological surveillance (*54*) and pathogen transmission modeling (*45*).

REFERENCES AND NOTES

1. N. Zhu *et al.*, *N. Engl. J. Med.* **382**, 727–733 (2020).
2. T. Hale *et al.*, *Nat. Hum. Behav.* **5**, 529–538 (2021).
3. L. Rodgers *et al.*, *Clin. Infect. Dis.* **73** (Suppl 1), S110–S117 (2021).
4. K. Hirae, T. Hoshina, H. Koga, *Int. J. Infect. Dis.* **128**, 265–271 (2023).
5. J. Hatoun, E. T. Correa, S. M. A. Donahue, L. Vernacchio, *Pediatrics* **146**, e2020006460 (2020).
6. A. Ullrich *et al.*, *Lancet Reg. Health Eur.* **6**, 100103 (2021).
7. J. A. McBride, J. Eickhoff, E. R. Wald, *Pediatr. Infect. Dis. J.* **39**, e449–e452 (2020).
8. M. J. Geng *et al.*, *Nat. Commun.* **12**, 6923 (2021).
9. S. Matczak *et al.*, *Euro Surveill.* **27**, 2100933 (2022).
10. E. Tessier *et al.*, *BMC Public Health* **22**, 405 (2022).
11. R. E. Baker *et al.*, *Proc. Natl. Acad. Sci. U.S.A.* **117**, 30547–30553 (2020).
12. M. W. Fong, N. H. L. Leung, B. J. Cowling, P. Wu, *Emerg. Infect. Dis.* **27**, 1525–1527 (2021).
13. K. Messacar *et al.*, *Lancet* **400**, 1663–1665 (2022).
14. A. G. Feldman, S. T. O'Leary, L. Danziger-Isakov, *Clin. Infect. Dis.* **73**, 1920–1923 (2021).
15. D. N. Durrheim *et al.*, *Nat. Med.* **27**, 360–361 (2021).
16. A. Handel, I. M. Longini Jr., R. Antia, *Proc. Biol. Sci.* **274**, 833–837 (2007).
17. T. D. Hollingsworth, D. Klinkenberg, H. Heesterbeek, R. M. Anderson, *PLOS Comput. Biol.* **7**, e1001076 (2011).
18. E. Rios-Guzman *et al.*, *Nat. Commun.* **15**, 3374 (2024).
19. C. Rodrigues *et al.*, *Euro Surveill.* **29**, 2400459 (2024).
20. K. Causey *et al.*, *Lancet* **398**, 522–534 (2021).
21. R. Moynihan *et al.*, *BMJ Open* **11**, e045343 (2021).
22. C. Arsenault *et al.*, *Nat. Med.* **28**, 1314–1324 (2022).
23. P. Rohani, C. J. Green, N. B. Mantilla-Beniers, B. T. Grenfell, *Nature* **422**, 885–888 (2003).
24. D. A. Vasco, H. J. Wearing, P. Rohani, *J. Theor. Biol.* **245**, 9–25 (2007).
25. J. A. Hay *et al.*, *Science* **373**, eabh0635 (2021).
26. R. E. Baker *et al.*, *Nat. Rev. Microbiol.* **20**, 193–205 (2022).
27. C. M. Zipfel, V. Colizza, S. Bansal, *Vaccine* **39**, 3645–3648 (2021).
28. S. S. Lee, C. Viboud, E. Petersen, *Int. J. Infect. Dis.* **122**, 1002–1004 (2022).
29. Z. Zheng, V. E. Pitzer, E. D. Shapiro, L. J. Bont, D. M. Weinberger, *JAMA Netw. Open* **4**, e2141779–e2141779 (2021).
30. D. A. Kalkowska *et al.*, *Vaccine* **41** (Suppl 1), A12–A18 (2023).
31. C. F. McQuaid *et al.*, *Eur. Respir. J.* **56**, 2001718 (2020).
32. L. Cilloni *et al.*, *EClinicalMedicine* **28**, 100603 (2020).
33. M. Briga, E. Goult, T. S. Brett, P. Rohani, M. Domenech de Cellès, *Nat. Commun.* **15**, 921 (2024).
34. H. He *et al.*, *Vaccine* **40**, 6956–6962 (2022).
35. S. W. Park *et al.*, *Epidemics* **46**, 100736 (2024).
36. US Centers for Disease Control and Prevention (CDC), NNDSS Data Tables [Internet]. 2023. Available from: https://data.cdc.gov/browse?q=NNDSS
37. Centers for Disease Control & Prevention, Weekly U.S. Influenza Surveillance Report 2024; https://www.cdc.gov/fluview/index.html [cited 11 February 2024].
38. M. A. Foster *et al.*, *MMWR Morb. Mortal. Wkly. Rep.* **68**, 413–415 (2019).
39. X. Ma *et al.*, *J. Am. Vet. Med. Assoc.* **260**, 1157–1165 (2022).
40. K. H. Brodersen, F. Gallusser, J. Koehler, N. Remy, S. L. Scott, *Ann. Appl. Stat.* **9**, 247 (2015).
41. D. M. Weinberger *et al.*, *JAMA Intern. Med.* **180**, 1336–1344 (2020).
42. D. J. Earn, P. Rohani, B. M. Bolker, B. T. Grenfell, *Science* **287**, 667–670 (2000).
43. D. A. Salmon, M. Z. Dudley, J. M. Glanz, S. B. Omer, *Vaccine* **33** (suppl. 4), D66–D71 (2015).
44. A. Sasaki, S. Lion, M. Boots, *Nat. Ecol. Evol.* **6**, 51–62 (2022).
45. D. V. Gokhale, T. S. Brett, B. He, A. A. King, P. Rohani, *Proc. Natl. Acad. Sci. U.S.A.* **120**, e2207595120 (2023).
46. T. S. Brett, P. Rohani, *PNAS Nexus* **1**, pgac159 (2022).
47. T. Bedford *et al.*, *Nature* **523**, 217–220 (2015).
48. Z. Chen *et al.*, *Science* **386**, eadq3003 (2024).
49. J. Piret, G. Boivin, *Emerg. Infect. Dis.* **28**, 273–281 (2022).
50. B. Manuelpillai, B. Lopman, C. R. Doran, C. Porter, *J. Infect. Dis.* **231**, e1075–e1079 (2025).
51. K. Nelson, B. Lopman, *Science* **377**, 33–34 (2022).
52. A. C. Perofsky *et al.*, *Nat. Commun.* **15**, 4164 (2024).
53. H. G. Nijhuis, L. J. G. van der Maesen, *Int J Soc Qual.* **11**, v–xx (2021).
54. C. J. E. Metcalf *et al.*, *Lancet* **388**, 728–730 (2016).
55. T. Hastie, R. Tibshirani, J. H. Friedman, *The Elements of Statistical Learning: Data Mining, Inference, and Prediction* (Springer, 2009), vol. 2.
56. P. J. Rousseeuw, *J. Comput. Appl. Math.* **20**, 53–65 (1987).
57. T. Brett, Data for: Collateral effects of COVID-19 pandemic control on the US, Zenodo (2025); https://doi.org/10.5281/zenodo.16772531.

ACKNOWLEDGMENTS

We thank B. Grenfell and the Rohani lab for comments on this work. **Funding:** National Institutes of Health (R21AI171509 (P.R., T.B.). National Institute of Allergy and Infectious Diseases, National Institutes of Health, Department of Health and Human Services, under contract no. 75N93021C00018 (NIAID Centers of Excellence for Influenza Research and Response, CEIRR) (P.R.). **Author contributions:** Conceptualization: T.B., P.R. Methodology: T.B., P.R. Investigation: T.B. Visualization: T.B. Funding acquisition: P.R. Project administration: P.R. Supervision: P.R. Writing – original draft: T.B. Writing – review & editing: T.B., P.R. **Competing interests:** The authors declare that they have no competing interests. **Data and materials availability:** All data and code to reproduce results have been deposited in Zenodo (*57*) (https://doi.org/10.5281/zenodo.16772531). **License information:** Copyright © 2025 the authors, some rights reserved; exclusive licensee American Association for the Advancement of Science. No claim to original US government works. https://www.sciencemag.org/about/science-licenses-journal-article-reuse

SUPPLEMENTARY MATERIALS

science.org/doi/10.1126/science.adw4964
Materials and Methods; Figs. S1 to S22; Tables S1 and S2; References (*58*–*71*);
MDAR Reproducibility Checklist

Submitted 5 February 2025; accepted 8 August 2025

10.1126/science.adw4964